Published in final edited form as:
Am J Physiol Heart Circ Physiol. 2007 March ; 292(3): H1607–H1618. doi:10.1152/ajpheart.00525.2006.

Cellular and Molecular Determinants of Altered Ca^{2+} Handling in the Failing Rabbit Heart:

Primary Defects in SR Ca^{2+} Uptake and Release Mechanisms

Antonis A Armoundas, PhD[*], **Jochen Rose, MD**[*], **Rajesh Aggarwal, PhD**, **Bruno D Stuyvers, PhD**, **Brian O'Rourke, PhD**, **David A. Kass, MD**, **Eduardo Marbán, MD PhD**, **Stephen R. Shorofsky, MD, PhD**, **Gordon F. Tomaselli, MD**[#], and **C. William Balke, MD**
From the Cardiovascular Research Center, Massachusetts General Hospital, Harvard Medical School, Charlestown, MA (AAA), the Department of Medicine, Division of Molecular Cardiobiology, Johns Hopkins University, Baltimore, MD (JR, BO'R, DAK, EM, GFT), the Department of Medicine, Division of Cardiology (SRS, RA), University of Maryland, Baltimore, MD, the Department of Medicine, Division of Cardiology (BDS) University of Calgary, Canada, and the Departments of Medicine and Physiology and the Institute of Molecular Medicine, University of Kentucky College of Medicine, Lexington, KY (CWB).

Abstract

Myocytes from the failing myocardium exhibit depressed and prolonged Ca^{2+} transients ($[Ca^{2+}]_i$ transients) that are, in part, responsible for contractile dysfunction and unstable repolarization. In order to better understand the molecular basis of the aberrant Ca^{2+} handling in heart failure (HF), we studied the rabbit pacing tachycardia HF model. Induction of HF was associated with AP duration prolongation that was especially pronounced at low stimulation frequencies. The L-type calcium channel current ($I_{Ca,L}$) density (−0.964±0.172 vs. −0.745±0.128 pA/pF at +10 mV) and NCX (2.1 ±0.8 vs. 2.3±0.8 pA/pF at +30 mV) currents were not different in myocytes from control and failing hearts. The amplitude of peak $[Ca^{2+}]_i$ was depressed (at +10 mV, 0.72±0.07 μM and 0.56±0.04 μM in normal and failing hearts correspondingly, $p<0.05$) with slowed rates of decay and reduced Ca^{2+} spark amplitudes ($p<0.0001$) in myocytes isolated from failing compared to control hearts. Inhibition of sarcoplasmic reticulum Ca^{2+}-ATPase (SERCA2a) revealed a greater reliance on NCX to remove cytosolic Ca^{2+} in myocytes isolated from failing compared to control hearts ($p<0.05$). The mRNA levels of the α_{1C} subunit, ryanodine receptor (RyR) and NCX were unchanged from controls, while SERCA2a and phospholamban (PLB) were significantly down regulated in the failing compared with the control hearts ($p<0.05$). α_{1C} protein levels were unchanged, RyR, SERCA2a and PLB were significantly down regulated ($p<0.05$), while NCX protein was significantly up regulated ($p<0.05$). These results support a prominent role for the sarcoplasmic reticulum in the pathogenesis of HF, in which abnormal SR Ca^{2+} uptake and release synergistically contribute to the the depressed $[Ca^{2+}]^i$ and the altered action potential profile phenotype.

Introduction

The reduced contractility and altered repolarization of the failing human heart and many animal models of heart failure (HF) are, in part, the result of abnormal intracellular Ca^{2+} cycling (4, 34,35,57,58,66). However, despite extensive investigation, the precise molecular mechanisms

#Correspondence to: Gordon F. Tomaselli, M.D., Johns Hopkins University, Division of Cardiology, 844 Ross Building, 720 Rutland Avenue, Baltimore, MD 21205, Phone: (410) 955-2774, Fax: (410) 502-2096, E-mail: E-mail: gtomasel@jhmi.edu.
*These authors contributed equally

responsible for altered Ca^{2+} handling in the failing heart remain controversial. Although there is a general consensus that sarcoplasmic reticulum (SR) Ca^{2+} handling is abnormal in HF, some studies suggest these abnormalities are primarily the result of the abnormal density/function of Ca^{2+} uptake and extrusion mechanisms (i e, SR Ca^{2+}-ATPase, SERCA2a and Na^{+}-Ca^{2+} exchanger, NCX) (34,66) while others attribute these abnormalities primarily to alterations in SR Ca^{2+} release (via the SR Ca^{2+} release channel, ryanodine receptor, RyR) (57,58,75). Furthermore, while the different animal models of HF exhibit a similar phenotype reminiscent of human HF, emerging information supports the notion that the common phenotype of HF may represent a final common pathway for unique model- (or injury-) specific molecular phenotypes.

The pacing-induced HF model is characterized by abnormal β-adrenergic receptor signaling (46) and elevated renin-angiotensin-aldosterone stimulation (56) that result in chamber dilation with markedly elevated diastolic pressures, depressed systolic function (83), and increased apoptosis (48). Thus, we hypothesized that in a pacing-induced HF model the altered autonomic tone results in abnormal SR Ca^{2+} release and related defects in SR Ca^{2+} uptake as the primary mechanism of abnormal Ca^{2+} homeostasis. In order to better understand the mechanisms responsible for abnormal Ca^{2+} homeostasis and cellular electrophysiology, we studied the L-type Ca current ($I_{Ca,L}$) and NCX currents, whole cell Ca^{2+} transients ($[Ca^{2+}]_i$), local Ca^{2+} transients (i.e. Ca^{2+} sparks), and mRNA and protein levels of the major Ca^{2+} handling molecules in the rabbit pacing -induced HF model.

In order to examine the hypothesis that the failing-myocyte phenotype, manifested by the depressed Ca^{2+} transients and potentially arrhythmogenic prolonged APD, is the result of a single versus a multiplicity of mechanisms, we employed a comprehensive approach to isolate and study the molecular and functional phenotype of potentially abnormal Ca^{2+} homeostatic processes, involving the primary Ca^{2+} entry, release, uptake and extrusion mechanisms in myocytes from failing hearts.

Methods

Rabbit pacing-induced heart failure model

Nine New Zealand rabbits of either sex underwent sterile implantation of a bipolar pacemaker. Rabbits were anesthetized with intravenous thiopental sodium, intubated and volume ventilated. A laparotomy was performed and the diaphragm and the pericardium were opened to expose the heart. Two custom-made pacing wires were placed in the apex of the heart. A VVI pacemaker (Minix 8340 or Thera SR 8962, Medtronic) was inserted into a pocket formed between the abdominal muscles. Rapid pacing was maintained by permanently attaching a magnet to the posterior surface of the pacemaker pulse generator. Animals were allowed to recover from surgery for 3 to 4 days, after which pacing was initiated at 400 bpm for 2 to 4 weeks. Heart failure was verified by transthoracic echocardiography. After 2.5±0.7 weeks of pacing, the left ventricular end-diastolic diameter increased (normal: 13±3 mm vs. failing: 18 ±3 mm; $p< 0.05$), left ventricular end-diastolic pressure increased (normal: 2.0±3 mm Hg vs. failing: 19.0±7.1 mm Hg; $p < 0.05$), systolic fractional shortening (in % of end-diastolic diameter) decreased (normal: 46±8 % vs. failing: 21±7 %; $p <0.05$) and the rate of pressure rise (dP/dt) decreased (normal: 6900±1620 mm Hg/s vs. failing: 3600±270 mm Hg/s; $p < 0.05$) consistent with severe HF (35). All procedures involving animals were approved by the Institutional Animal Care and Use Committee (IACUC) of the Johns Hopkins University.

Isolation of ventricular myocytes

Isolated myocytes were obtained from failing and control left ventricles by enzymatic dissociation as previously described (34,35). The apex (1–3 g) was excised and immediately

frozen in liquid nitrogen for later protein and mRNA analysis. Only Ca^{2+}-tolerant rod-shaped myocytes with clear cross striations and without spontaneous contractions or signification granulation were selected for experiments.

Solutions

The external solution for action potential (AP) measurements contained (in mmol/L): NaCl 138, KCl 4, $CaCl_2$ 2, $MgCl_2$ 1, glucose 10, NaH_2PO_4 0.33, and HEPES 10 (pH 7.4 with NaOH). The pipette solution for recording APs contained (in mmol/L): KCl 140, NaCl 5, $MgCl_2$ 1, HEPES 10, EGTA 2, and Mg-ATP 4 (pH 7.4 with KOH).

For the measurement of the $I_{Ca,L}$ and $[Ca^{2+}]_i$,the extracellular solution contained (in mmol/L): NaCl 140, dextrose 10, HEPES 10, CsCl 10, $MgCl_2$ 1, and $CaCl_2$ 1 (pH adjusted to 7.4 with NaOH). The intracellular solution contained (in mmol/L): Cs-glutamate 130, HEPES 10, $MgCl_2$ 0.33, Mg_2-ATP 4 and Indo-1 (Molecular Probes) 0.05 and the pH was adjusted to 7.2 with CsOH.

For the measurement of NCX current, the extracellular solution contained (in mmol/L): NaCl 140, $CaCl_2$ 2, $MgCl_2$ 2, HEPES 5, glucose 10 (pH=7.4, adjusted by NaOH). In addition, the Na^+-K^+-ATPase, K^+-channels, and Ca^{2+}-channels were blocked with 20 μmol/L ouabain, 1 mmol/L $BaCl_2$, and 1 μmol/L nifedipine, respectively. The electrogenic NCX current was inhibited by addition of 5 mmol/L Ni^{2+}. The pipette solution contained (in mmol/L): CsOH 146, NaCl 20, L-aspartic acid 42, $MgCl_2$ 3, HEPES 10, TEA 20, $CaCl_2$ 21, EGTA 42, and MgATP 10 (pH=7.4 adjusted by CsOH). The free Ca^{2+} concentration was 67 nmol/L (18).

$[Ca^{2+}]_i$ in the presence and absence of thapsigargin were measured in an extracellular solution containing (in mmol/L): NaCl 138, KCl 4, $MgCl_2$ 1, $CaCl_2$ 2, NaH_2PO_4 0.33, glucose 10 (pH=7.4, adjusted by NaOH). The pipette solution contained (in mmol/L): K glutamate 130, KCl 9, NaCl 10, $MgCl_2$ 0.5 and MgATP 5 (pH=7.2, adjusted by KOH) and 80 μmol/L indo-1.

Electrophysiological recording techniques

The whole-cell configuration of the patch-clamp technique was used. Myocytes were transferred to the stage of an inverted microscope and superfused with external solution at a rate of 1–2 mL/min. All recordings were performed at 37°C. Whole-cell currents were recorded using an Axopatch 200A amplifier (Axon Instruments), low-pass-filtered at 5 kHz and digitized at 10 kHz via a Digidata 1200 A/D (Axon Instruments) interface for off-line analysis. Myocyte capacitance was calculated by integrating the area under an uncompensated capacity transient elicited by a 10 mV depolarizing pulse from a holding potential of −80 mV.

A xenon arc lamp was used to excite indo-1 fluorescence at 365 nm and the ratio ($R=F_{405nm}/F_{495nm}$) of the emitted fluorescence after subtraction of cellular autofluorescence was used to calculate free $[Ca^{2+}]_i$ according to the equation $[Ca^{2+}]_i = K_d \times \beta[(R-R_{min})/(R_{max}-R)]$, using a K_d of 844 nmol/L, as reported for rabbit cardiomyocytes (7). The average R_{min}, R_{max}, and β for the fluorescence system were determined to be 0.4±0.4, 9.8±2.9 and 7.8±3.2 (n=6) respectively, as previously described (66). The rate of Ca^{2+} removal (τ_{Ca}) was determined by fitting a single exponential to the $[Ca^{2+}]_i$ time course 20 msec after returning to the holding potential.

Local SR Ca^{2+} release events, Ca^{2+} sparks

Spontaneous Ca^{2+} sparks were recorded using the fluorescence of the Ca^{2+} indicator fluo-3 and a custom-built laser scanning confocal microscope (82). The bath solution was a modified Tyrode's solution containing (in mM): NaCl 135, CsCl 4, $NaHPO_4$ 0.33, $MgSO_4$ 1, HEPES 10, glucose 10, $CaCl_2$ 1, with pH 7.3. Myocytes were loaded with the membrane permeant

form of the Ca^{2+} indicator, fluo-3 AM (Molecular Probes, Eugene OR), by incubating the myocytes for 30 minutes at 21–23°C in the bath solution containing fluo-3 AM (10 μmol/L) and pleuronic acid (0.05% weight volume^{-1}). Fluo-3 was excited with an argon laser at a wavelength of 488 nm. The fluorescence emission was measured at wavelengths >515 nm.

The lateral and axial spatial resolutions of the confocal system equipped with a 63X 1.4 NA oil immersion objective lens, were 0.25 μm and 0.52μm. Line-scan images were created from a series of 512 lines with 256 pixels per line, 0.1 μm per pixel, and 3.0 ms per line (including 0.5 ms reset time per scan); the pixel dwell times were 10.0 μs. The scan line positions were selected to be in the middle of the myocyte away from the edges and avoiding the nucleus. Sparks were sampled in rabbit ventricular myocytes according to the protocol used by Satoh et al (71). Briefly, myocytes were field stimulated every 6s. Ca^{2+} sparks were determined from the line scan images and sampled during the resting period following the overall Ca^{2+} transient (Figure 3A). Amplitude, duration, and width (spread in the axial direction) were determined for each Ca^{2+} spark. Data from control were compared to that from failing animals using the Mann-Whitney test for comparison of non-normal distributions. The line scan images were analyzed using custom made IDL routines.

mRNA measurements

The DNA fragments used to generate rabbit-specific riboprobes were amplified from reverse-transcribed total rabbit ventricular RNA using the polymerase chain reaction (PCR). The PCR products were cloned into pCR2.1 (Invitrogen) and, if necessary, subcloned into the *EcoR1* site of pSP70 (Promega). All constructs were confirmed by DNA sequencing. The Na^+ channel template was designed to protect a fragment in the I-II linker of the Na^+ channel that is unique to the cardiac isoform.

The rabbit cardiac Na^+-channel (rabNav1.5) probe spans nucleotides 1655 to 1801 (146 bp) and NCX (rabNCX) spans nucleotides 443 to 585 (142 bp) (Table 1). For better discrimination of the fragment sizes, the probes were cut at the unique restriction sides (Ngom I for rabNav1.5, Bsa I for rabNCX), resulting in protected sequences of 78 bp and 116 bp for rabNav1.5 and rabNCX, respectively.

Ribonuclease protection assays (RPAs) were performed as previously described (39). Total RNA was prepared using TRIzol reagent (GIBCO) according to the manufacturer's instructions. The integrity of all RNA samples was confirmed by analysis on a denaturing agarose gel and quantified by optical density measurements at 260 nm. Determinations were performed in duplicate on 10 μg of RNA from each ventricular sample.

Steady-state mRNA levels were quantified by exposing the gels on a storage phosphor screen, then scanning on a phosphoimager (Molecular Dynamics); quantification of the transcript levels was performed using ImageQuant software (Molecular Dynamics). The level of the rabNCX gene expression is given as the relative density of the protected fragment normalized to the density of the control protected fragment (rabNav1.5), the cardiac isoform of the Na channel, thereby normalizing for both RNA loading and the fraction of the sample that is cardiac myocytes.

Fluorescence-based kinetic real-time PCR was performed using a Perkin-Elmer Applied Biosystems Model 7900 sequence-detection system to quantify mRNA levels as previously described (14). Total RNA was isolated from the rabbit ventricle using Qiagen RNeasy with on-column DNase digestion. Each reporter signal is then divided by the fluorescence of an internal reference dye (ROX) to normalize for non–PCR-related fluorescence and to 18S rRNA to normalize for loading. All primers and probes are shown in Table 1. The level of gene expression was normalized to a reference sample to permit comparison among samples.

Protein measurements

Quantification of SERCA2, PLB and NCX proteins was performed as previously described (14). Frozen tissue samples were homogenized on ice in 10 mL/gm of tissue (weight weight) in lysis buffer containing (in mmol/L): NaCl 145, MgCl2 0.1, HEPES 15, and EGTA 10 (pH=7.0), and protease inhibitors (Complete™, Boehringer Mannheim). The protein concentration was assayed with Protein-Assay™ (Bio-Rad). Quantification of RyR was performed on membrane preparations as previously described (58). For separation of SERCA2a, PLB and NCX, lysates were run in triplicate on a 4–15% polyacrylamide gradient gel (Bio-Rad) and for RyR membrane preparations were run on 3–8% Tris-Acetate gel (Invitrogen). The same control sample was run on every gel to be used as a reference for normalization across blots. Non-specific antibody binding was blocked for one hour in phosphate-buffered saline (PBS) with Tween-20 and nonfat milk, then the membranes were incubated in Tween/PBS with the primary antibodies (Alomone Labs: polyclonal anti-Ca channel α1c antibody, ACC-003; Affinity BioReagents: monoclonal anti-SERCA2a antibody, MA3-910, monoclonal anti-phospholamban antibody, MA3-922, monoclonal anti-NCX antibody, MA3-926 and monoclonal anti-RyR antibody, MA3-916) by incubation with the appropriate horseradish peroxidase-conjugated secondary antibody. Proteins were detected using chemiluminescence on hyperfilm-ECL (Amersham Life Science) or Lumi-Light Western Blotting Substrate (Roche).

Films were digitally scanned, band densities were normalized to the average density of the reference lanes.

Statistical analysis

Pooled electrophysiological data are presented as mean ± SE while protein and mRNA as mean ± SD. Statistical comparisons were made using unpaired t-tests (unless otherwise specified), with $p<0.05$ considered to be statistically significant.

Results

Action potential duration in control and failing myocardium

We measured the APD at 50 and 90% repolarization (APD_{50} and APD_{90}) from 18 myocytes isolated from 12 control ventricles and 11 myocytes from 5 failing ventricles over a range of stimulation frequencies from 0.1 to 1.0 Hz. The APD_{50} and APD_{90} of myocytes isolated from the midmyocardial layer of failing hearts were significantly longer than those of isolated from normal hearts at stimulation frequencies of 0.1 and 0.2 Hz (Figures 1A and 1B). The resting membrane potential was not significantly different in myocytes isolated from failing compared to control hearts (−86.8± 6.7 mV in control vs −87.7± 2.9 mV in failing hearts at 1 Hz).

Measurement of the $I_{Ca,L}$, $[Ca^{2+}]_i$ transients and sparks

Contraction in the ventricular myocardium is initiated by Ca^{2+} entry through the $I_{Ca,L}$. Representative $[Ca^{2+}]_i$ transients from control and failing hearts, elicited by voltage steps to −40, −20, 0, 20 and 40 mV from a holding potential of −100 mV with a pre-pulse to −50mV to inactivate the Na^+ current are shown in Figure 2A. The voltage dependence and kinetics of $I_{Ca,L}$, do not differ between myocytes isolated from control and failing hearts. The current-voltage (I–V) relationships for $I_{Ca,L}$ measured in ventricular myocytes isolated from control and failing hearts reveals no significant difference in the $I_{Ca,L}$ density (Fig 2C).

In contrast, the peak $[Ca^{2+}]_i$ in myocytes isolated from failing hearts are significantly depressed at test voltages greater than or equal to 0 mV (Fig. 2B). To investigate whether changes in the $[Ca^{2+}]_i$ transient amplitude are related to changes in local Ca^{2+} release events we measured spontaneous Ca^{2+} sparks. Representative Ca^{2+} sparks measured in myocytes isolated from

control and failing hearts are shown in Figure 3B. The amplitudes of the Ca^{2+} sparks are reflected in the ratio of the peak to background fluorescences and analyzed using the distribution histograms shown in Figure 3C. Ca^{2+} sparks in myocytes from the failing hearts are significantly smaller than those from control hearts ($p<0.0001$, Mann-Whitney test of medians). There were no differences in Ca^{2+} spark kinetics (i.e., width or duration) in cells isolated from control and failing animals (1.1 ± 0.7 vs 1.0 ± 0.8 μm and 22.6 ± 11.8 vs 22.4 ± 13.8 ms, respectively). Finally, there was no difference in the Ca^{2+} spark frequency (obtained by dividing each of the histograms of Figure 3B by its corresponding number of frames) between the two myocyte groups (Figure 3D), albeit the distribution corresponding to the failing myocytes appears to be smaller.

Measurement of the Na^{+}-Ca^{2+} exchanger current

NCX significantly contributes to the $[Ca^{2+}]_i$ and AP profile. We measured the NCX current using the voltage protocol shown in Figure 4A. Ramp-wise changes in voltage (+60 to −120 mV, 90 mV/s) were applied at a rate of 0.1 Hz from a holding potential of −30 mV. Under the experimental conditions used, the Ni^{2+}-sensitive current is primarily through the exchanger (44). Figures 4B and 4C show representative current recordings in myocytes isolated from a control and a failing heart, respectively. After application of 5 mmol/L Ni^{2+}, the current decreased (tracing b) compared to that in the absence of Ni^{2+} (tracing a). The difference currents (a–b) are shown in the bottom panels respectively. As demonstrated in the representative recordings and as summarized in Figure 4D and Table 2, there was no significant difference in the NCX current density in myocytes isolated from control and failing hearts. The reversal potentials did not differ between myocytes isolated from control and failing hearts (-28.7 ± 5.2 mV vs. -30.1 ± 5.0 mV); both values were close to the calculated value of −27.2 mV, consistent with the Ni^{2+}-sensitive current representing NCX current and indicating effective buffering of intracellular Ca^{2+} under our experimental conditions (Table 2).

Measurement of the decay of the $[Ca^{2+}]_i$ transient

The contribution of NCX to Ca^{2+} removal was assessed by measurement of $[Ca^{2+}]_i$ in the presence and absence of the SERCA2a inhibitor, thapsigargin. $[Ca^{2+}]_i$ transients were elicited by 200 ms voltage-clamp steps to +20 mV from a holding potential of −80 mV at a rate of 0.5 Hz before and 3 minutes after exposure to 10 μmol/L thapsigargin.

As illustrated in Figure 5A, thapsigargin reduced the amplitude and prolonged the decay of the $[Ca^{2+}]_I$ transient. The $[Ca^{2+}]_i$ transients in the myocytes isolated from the failing ventricles (Fig. 5B) were characterized by smaller peak amplitudes and slower decays compared to the myocytes isolated from control hearts. Thapsigargin further reduced the peak and prolonged the decay of $[Ca^{2+}]_i$ transients of the myocytes from failing hearts. In the baseline state, the time constant of decay of $[Ca^{2+}]_i$ (τ_{Ca}) was significantly larger in myocytes isolated from failing myocardium. After inhibition of SERCA2a, τ_{Ca} was comparable in myocytes from both groups (Fig. 5C). The absolute increase in τ_{Ca} was greater in myocytes isolated from the control hearts but this difference did not reach statistical significance (Fig. 5D). The *relative* increase in τ_{Ca} with thapsigargin, however, was significantly larger in myocytes isolated from control compared to failing hearts ($p<0.05$, Fig. 5D). This result suggests that myocytes from failing hearts rely more on NCX for cytosolic Ca^{2+} removal than myocytes isolated from control hearts consistent with a defect in SR Ca^{2+} uptake.

Measurement of Ca^{2+} handling mRNA and protein

We measured mRNA and immunoreactive protein levels of the major Ca^{2+} handling proteins to better understand the molecular mechanisms of altered excitation-contraction coupling (ECC) in this model of HF.

The $I_{Ca,L}$ α_{1c} subunit, RyR, SERCA2a and phospholamban mRNA levels were measured using kinetic RT-PCR (Figure 6B). There was no significant difference of the level of α_{1c} (Fig. 6A) or RyR (Fig. 6B) mRNA in ventricular myocardium from control and failing hearts. However, the mRNA levels of the SERCA2a (Fig. 6C) and PLB (Fig. 6D) were significantly reduced in failing compared with control hearts ($p<0.05$).

NCX mRNA was quantified by RPA, figure 6E shows a representative RPA comparing left ventricular apical samples from normal and failing hearts. There is sample to sample variation in both normal and failing hearts in the rabNCX as well as the rabNav1.5 protected fragments; however, the summarized data (Fig. 6F) reveals no significant difference in the steady-state level of NCX mRNA in failing as compared to control myocardium.

Western blotting was used to measure the levels of immunoreactive Ca^{2+} handling proteins. We observed no difference in the level of the α_{1c} protein expression (Fig. 7A) in tissues from control and failing hearts. There was a modest but statistically significant down regulation of the level of RyR (Fig. 7B), SERCA2a (Fig. 7C) and PLB monomer (Fig. 7D) proteins in failing compared with control ventricles. The antibody used in the NCX Western blots recognized 3 specific bands of ~160, ~120, and ~70 kDa (23), there is a 48% overall increase in immunoreactive protein in failing myocardium (Figure 7E, $p < 0.05$).

Discussion

The pacing tachycardia heart failure model typically yields dilated hearts, with depressed basal contractility and elevated diastolic pressures. Other dominant features of this model include a marked decline in systolic function, chamber dilation, a marked increase in end-diastolic pressure and chamber remodeling. This model is also characterized by abnormal β-adrenergic receptor signaling (46), elevated activity of the renin-angiotensin-aldosterone pathway (56), apoptosis (48) and atrial and ventricular arrhythmias (67). Therefore, this model recapitulates the phenotype of certain types of human HF manifested by depressed $[Ca^{2+}]_i$ transients and prolonged APs.

The overall goal of this study was to probe the mechanism(s) responsible for the altered Ca^{2+} homeostasis and cellular electrophysiology in a clinically relevant rabbit model of HF. We found that in myocytes from failing hearts the APD is longer and the $I_{Ca,L}$ density and Na^+-Ca^{2+} exchanger (NCX) currents were unaltered, yet the Ca^{2+} spark amplitude and $[Ca^{2+}]_i$ transients were smaller. Decay of $[Ca^{2+}]_i$ in myocytes isolated from control hearts exhibited a greater reliance on SR Ca^{2+} uptake, consistent with aberrant uptake in cells from failing hearts (Figure 5). At the molecular level, we found that in the failing heart the SERCA2a and phospholamban (PLB) mRNA levels were down regulated as well as the RyR, SERCA2a and PLB protein levels while the NCX protein was up regulated. Overall, our data suggest that the development of HF in this model is associated with interrelated defects in both SR Ca^{2+} uptake and release mechanisms which synergistically contribute to the phenotype observed in myocytes from failing hearts.

Trigger of SR Ca^{2+} release

Compared with controls, we did not find any significant changes in the Ca^{2+} trigger for SR Ca^{2+} release in this model, namely there was no significant reductions in $I_{Ca,L}$ density (Fig. 2C), mRNA (Fig. 6A) and in the immunoreactive α_{1C} subunit (Fig. 7A).

Our data are entirely consistent with those in the canine pacing-induced HF model (40,65) human dilated cardiomyopathy (DCM) and ischemic cardiomyopathy (ICM) (8,9,60,69), all of which exhibit no change in the $I_{Ca,L}$ density. However, some studies in the rabbit pacing-induced (80) and rat post myocardial infarction (54) HF models have shown a reduction in the

$I_{Ca,L}$ density and studies in human DCM and ICM have shown a frequency dependent decrease in the $I_{Ca,L}$ density (77). Also, studies in human DCM and ICM (27,79,80), the rabbit pacing-induced HF model (12) and the rat (17) and canine (24) post-MI HF models have shown a decrease of the dihydropyridine (DHP) binding sites, however they were found unaltered in the canine pacing-induced HF model (81). The α_{1c} steady state mRNA level in the canine pacing-induced HF model (41) and the failing human heart have been reported to be unaltered (72), while it was found decreased in another study in the failing human heart (79).

Overall, it appears that differences among studies in the density of the $I_{Ca,L}$ or number of DHP binding sites can be attributed to differences in the severity of hypertrophy or failure.

SR Ca^{2+} release

In this study, we have observed that the decrease in $[Ca^{2+}]_i$ (Fig 2B and 5B) occurs despite the lack of a change in the trigger for Ca^{2+} release, the L-type Ca^{2+} current. There are several possible scenarios that could explain the depressed $[Ca^{2+}]_i$ at the level of SR Ca^{2+} release.

Experiments in ventricular myocytes (10,50), membrane vesicles reconstituted in planar lipid bilayers (11) and isolated cardiac membrane vesicles (36) have demonstrated that *SR lumen* Ca^{2+} influences RyR gating such that RyRs are more likely to be triggered by cytosolic Ca^{2+} when SR luminal Ca^{2+} is elevated, thus the decrease in SR Ca^{2+} content (or the elevation of the activation threshold of RyR2 for luminal and/or cytosolic Ca^{2+}) in the failing heart (34) could explain the reduction in Ca^{2+} release (Fig. 5). Alternatively, abnormal SR Ca^{2+} release could be attributed to RyR down regulation (Fig. 7B), or the ECC gain could be decreased in the failing myocytes. The role of the RyR in defective Ca^{2+} handling in the failing heart has been controversial at both the levels of expression (25,38,62) and function (38,57). Although we found no significant difference in the steady state levels of RyR mRNA (Fig. 6B) between control and failing hearts, the protein level of RyR was significantly down regulated in the failing hearts (Fig. 7B), suggesting that the down regulation of immunoreactive protein is not transcriptionally mediated in this model. On the other hand, while decreases in the ECC gain have been reported in failing rodent hearts (26), this observation has not been confirmed in large animal models (34) or in human (51) HF studies.

Overall, the net result of the above scenarios would be smaller Ca^{2+} spark amplitude and depressed $[Ca^{2+}]_i$ in myocytes from failing hearts. Ca^{2+} sparks in myocytes from failing human hearts are characterized by a slower time to peak and half-time of decay and larger full-width-at-half-maximum, compared to control hearts (53). In contrast to our previous findings in the hypertrophic heart (76), Ca^{2+} sparks in myocytes isolated from the failing rabbit ventricle are smaller compared to the control heart ($p<0.0001$), although the kinetics of the individual sparks were unchanged. Furthermore, we have shown that while the decreased $[Ca^{2+}]_i$ can be predominantly attributed to smaller Ca^{2+} spark amplitude, a non-significant decrease in the Ca^{2+} spark frequency (Fig. 3D) could synergistically contribute to smaller $[Ca^{2+}]_i$. The reduced frequency of sparks in myocytes from failing rabbit hearts is concordant with recently-published data in human myocytes (53). It is also important to note that the hypertrophy-related (76) increases in Ca^{2+} spark amplitudes occurred without changes in SR Ca^{2+} content.

We did not directly measure the Ca^{2+} content of the SR in this study and this is a potential limitation when comparing $[Ca^{2+}]_i$ and Ca^{2+} sparks between the two groups. However, we do not believe that changes in SR Ca^{2+} content between control and failing myocytes can entirely explain our results for the following reasons. Firstly, as noted above, hypertrophy-related increases in Ca^{2+} spark amplitudes occurred without significant changes in SR calcium content. Secondly, our experimental conditions, namely the low stimulation frequency and prepulses, were chosen specifically to minimize any potential changes in SR Ca^{2+} content and to insure a uniform, although not equal SR Ca^{2+} load. Lastly, differences in the $[Ca^{2+}]_i$ were observed

at low stimulation frequencies when there is no difference in the SR Ca^{2+} load between myocytes from normal and failing hearts (75). Therefore, while we cannot entirely exclude the possibility that differences in SR Ca^{2+} load between myocytes from normal and failing hearts contribute to our observed changes in the $[Ca^{2+}]_i$ and Ca^{2+} spark amplitude, we believe that defects in SR Ca^{2+} release independently contribute to the altered Ca^{2+} handling in this model.

Cytosolic Ca^{2+} removal

Our data are consistent with HF-associated changes in Ca^{2+} handling (5,8,66) manifested by a reduction in the amplitude of the $[Ca^{2+}]_i$ (Figures 2C and 5B). We have observed a significant reduction in the SERCA2a (Fig. 6C) and PLB (Fig. 6D) mRNA levels, with unaltered NCX mRNA level. We also observed a reduction in SERCA2a protein (Fig. 7C) (31,66) and PLB (Fig. 7C) protein levels and a significant up regulation of the NCX protein level.

Despite agreement that Ca sequestration by the SR is defective in the failing myocardium there is significant controversy about the molecular mechanisms. SERCA2a mRNA is decreased in a rat hypertrophy model (20), human DCM and ICM (2,20,22,28,47,52,59,73,78,79,85), but some studies of human DCM have shown no change of the SERCA2a mRNA (63,73,74). Fewer studies have shown a reduction in the immunoreactive protein in the rat, rabbit and canine post-MI HF models (13,28,31,45,66,85), while some studies of human DCM have shown no change of the SERCA2a protein (63,73,74).

Indeed a decrease in the SERCA2a to PLB ratio has been associated with defective Ca^{2+} handling and contraction in several models of cardiac hypertrophy and failure (29,30,37,61). While we found that the SERCA to PLB mRNA ratio was significantly decreased compared to controls (1.71 ± 0.46 versus 2.37 ± 0.65, $p < 0.05$) the ratio of SERCA2a to PLB protein did not change between the two groups (1.08 ± 0.29 and 0.93 ± 0.16, respectively). Therefore, we cannot attribute the changes in Ca^{2+} handling we observed in our model to changes in the SERCA2a/PLB protein ratio.

NCX constitutes the primary mode of extrusion of Ca^{2+} from the myocyte and is critically important to Ca^{2+} handling in the normal and failing heart. In the rabbit pacing-induced HF model, NCX protein is significantly increased (Fig. 7E). This is qualitatively and quantitatively consistent with previous reports in failing human hearts from patients with ICM (21,78) or DCM (70) and the canine pacing-induced (3,35,66) and rat post MI (54) HF models. However, the increase in NCX protein was not associated with a change in the level of mRNA, in contrast to other studies (68,84), which may be explained by altered turnover resulting in an increase in NCX protein.

Overall, our data support the conclusion that the abnormalities of Ca^{2+} handling that we observed in the rabbit rapid pacing model of heart failure can be attributed mainly to proximate abnormalities of the SR Ca^{2+} release mechanism that is further exacerbated by reduced SR Ca^{2+} uptake, for the following reasons. Firstly, we observed changes in the peak amplitudes of $[Ca^{2+}]_i$ transients (Figure 2B) rather than changes in decay rates (Figure 5D). Secondly, we observed decreases in the amplitudes of Ca^{2+} sparks under conditions where differences in the Ca^{2+} content of the SR are predicted to be small (75). And thirdly, we found a down regulattion of the RyR, SERCA2a and PLB protein2, but an unaltered SERCA2a/PLB protein ratio and unchanged NCX current density.

Summary and significance

The heart failure literature is replete with multiple conflicting reports regarding the mechanisms that underlie the observed abnormalities in Ca^{2+} homeostasis, AP prolongation and predisposition to life threatening arrhythmias in both animal models of heart failure and in the

failing human heart. The differences between these conflicting reports reflect, in part, the fact that distinct molecular abnormalities converge to a common heart failure phenotype. Such molecular abnormalities are often the result of distinct and divergent “insults” and “injuries” to the myocardium, which may produce heart failure phenocopies. The differential “trigger” events seen in animal heart failure models parallel that seen in human heart failure of different etiologies. Thus, understanding the molecular mechanisms of these trigger events has important implications in the treatment of heart failure patients resulting from different etiologies. These differences are further compounded by species differences in the expression and function of major Ca^{2+} cycling molecules and by differences in the spatio-temporal progression and severity of the disease.

The findings of the present study support the notion that pacing-induced heart failure in the rabbit results from a distinct mixed mechanism (namely, prominent abnormalities in SR Ca^{2+} release and uptake) compared to heart failure that is a consequence of prolonged pressure and/or volume overload (where abnormalities in SR Ca^{2+} uptake predominate). These observations, then, challenge the “conventional wisdom” that cardiac hypertrophy and systolic dysfunction are two different “set points” on the continuous “slippery slope” of “cellular failure” that leads inexorably to symptomatic heart failure.

Therefore, this requires not only identifying the disease gene(s), but eventually connecting the gene(s) to molecular pathways that initiate, promote, suppress, and potentially reverse surrogate endpoints of the disease phenotype. Such a process is likely to clarify the distinction between true mechanisms and mere markers of heart failure, a distinction that has far-reaching preventive and therapeutic implications.

Study limitations

The single most important limitation of this study is the lack of direct information regarding the SR Ca^{2+} content. However, the fact that we observed only changes in the peak amplitude of $[Ca^{2+}]_i$ rather than in its decay rate, at low stimulation frequencies suggests no or minimal differences in the SR Ca^{2+} load among myocytes from normal and failing hearts. Furthermore, given that in slowly stimulated myocytes from normal and failing hearts the difference in SR Ca^{2+} content is minimized (75), we are inclined to believe that the SR Ca^{2+} content in the Ca^{2+} spark experiments, is very similar. Thus, it would not alter the interpretation of our results pertaining to the abnormal SR Ca^{2+} release, even if the SR Ca^{2+} content is profoundly reduced in these myocytes.

In the present study the whole-cell patch clamp technique was used to measure L-type Ca and NCX current densities. The whole-cell patch clamp technique permits direct measurement of the currents in an intact cardiac myocyte however, this method will alter the cytosolic composition. Although, this artifact is equally applied to both control and failing myocytes, we cannot exclude the possibility that the Ca and NCX currents are differentially modulated by cytoplasmic mediators in control and failing myocardium (15,16).

Furthermore, in the experiments to measure the NCX current density the intracellular Ca^{2+} concentration was clamped by a high concentration of EGTA in the pipette solution. Ca^{2+} is an important regulator of the activity of the NCX (33,35) mediated by a high-affinity Ca^{2+} binding site composed of acidic residues in the large intracellular loop of the NCX (49). Since this Ca^{2+} affinity site is intrinsic to the NCX, it is unlikely that a difference in current density of the NCX between myocytes isolated from control and failing hearts would become apparent at higher intracellular Ca^{2+} concentrations. However, our data do not rigorously exclude this possibility.

Acknowledgements

We would like also to thank Yanli Tian, MD, Debbie DiSilvestre, Richard Tunin, for their technical support and Steven Reiken, PhD and Andrew R Marks, MD for advice in performance of the RyR protein quantification.

This work was supported by the NIH P50 HL 52307 (GFT, DAK, BOR, EM). Support was also provided by NIH 2RO1HL50435, 1RO1HL071865 (CWB), an Established Investigator Award (C9740089N) (CWB), an American Heart Association: Beginning Grant-in-Aid (#0365304U) (AAA), and a Scientist Development Grant (#0635127N) (AAA).

References

1. Ai X, Curran JW, Shannon TR, Bers DM, Pogwizd SM. Ca2+/calmodulin-dependent protein kinase modulates cardiac ryanodine receptor phosphorylation and sarcoplasmic reticulum Ca2+ leak in heart failure. Circ Res 2005;97:1314–1322. [PubMed: 16269653]
2. Arai M, Alpert NR, MacLennan DH, Barton P, Periasamy M. Alterations in sarcoplasmic reticulum gene expression in human heart failure. A possible mechanism for alterations in systolic and diastolic properties of the failing myocardium. Circulation Research 1993;72:463–469. [PubMed: 8418995]
3. Armoundas AA, Hobai IA, Tomaselli GF, Winslow RL, O'Rourke B. Role of sodium-calcium exchanger in modulating the action potential of ventricular myocytes from normal and failing hearts. Circ Res 2003;93:46–53. [PubMed: 12805237]
4. Armoundas AA, Wu R, Juang G, Marban E, Tomaselli GF. Electrical and structural remodeling of the failing ventricle. Pharmacol Ther 2001;92:213–230. [PubMed: 11916538]
5. Bailey BA, Dipla K, Li S, Houser SR. Cellular basis of contractile derangements of hypertrophied feline ventricular myocytes. J Mol Cell Cardiol 1997;29:1823–1835. [PubMed: 9236137]
6. Balijepalli RC, Lokuta AJ, Maertz NA, Buck JM, Haworth RA, Valdivia HH, Kamp TJ. Depletion of T-tubules and specific subcellular changes in sarcolemmal proteins in tachycardia-induced heart failure. Cardiovasc Res 2003;59:67–77. [PubMed: 12829177]
7. Bassani JW, Bassani RA, Bers DM. Calibration of indo-1 and resting intracellular [Ca]i in intact rabbit cardiac myocytes. Biophys J 1995;68:1453–1460. [PubMed: 7787031]
8. Beuckelmann DJ, Erdmann E. Ca(2+)-currents and intracellular [Ca2+]i-transients in single ventricular myocytes isolated from terminally failing human myocardium. Basic Res Cardiol 1992;87:235–243. [PubMed: 1497571]
9. Beuckelmann DJ, Nabauer M, Erdmann E. Intracellular calcium handling in isolated ventricular myocytes from patients with terminal heart failure. Circulation 1992;85:1046–1055. [PubMed: 1311223]
10. Cheng W, Kajstura J, Nitahara JA, Li B, Reiss K, Liu Y, Clark WA, Krajewski S, Reed JC, Olivetti G, Anversa P. Programmed myocyte cell death affects the viable myocardium after infarction in rats. Exp Cell Res 1996;226:316–327. [PubMed: 8806435]
11. Ching LL, Williams AJ, Sitsapesan R. Evidence for Ca(2+) activation and inactivation sites on the luminal side of the cardiac ryanodine receptor complex. Circ Res 2000;87:201–206. [PubMed: 10926870]
12. Colston JT, Kumar P, Chambers JP, Freeman GL. Altered sarcolemmal calcium channel density and Ca(2+)-pump ATPase activity in tachycardia heart failure. Cell Calcium 1994;16:349–356. [PubMed: 7859249]
13. Currie S, Smith GL. Enhanced phosphorylation of phospholamban and downregulation of sarco/endoplasmic reticulum Ca2+ ATPase type 2 (SERCA 2) in cardiac sarcoplasmic reticulum from rabbits with heart failure. Cardiovasc Res 1999;41:135–146. [PubMed: 10325961]
14. Deschenes I, DiSilvestre D, Juang GJ, Wu RC, An WF, Tomaselli GF. Regulation of Kv4.3 current by KChIP2 splice variants: a component of native cardiac I(to)? Circulation 2002;106:423–429. [PubMed: 12135940]
15. Despa S, Bers DM. Na/K pump current and [Na](i) in rabbit ventricular myocytes: local [Na](i) depletion and Na buffering. Biophys J 2003;84:4157–4166. [PubMed: 12770918]

16. Despa S, Islam MA, Weber CR, Pogwizd SM, Bers DM. Intracellular Na(+) concentration is elevated in heart failure but Na/K pump function is unchanged. Circulation 2002;105:2543–2548. [PubMed: 12034663]

17. Dixon IM, Lee SL, Dhalla NS. Nitrendipine binding in congestive heart failure due to myocardial infarction. Circ Res 1990;66:782–788. [PubMed: 2155068]

18. Fabiato A. Myoplasmic free calcium concentration reached during the twitch of an intact isolated cardiac cell and during calcium-induced release of calcium from the sarcoplasmic reticulum of a skinned cardiac cell from the adult rat or rabbit ventricle. J Gen Physiol 1981;78:457–497. [PubMed: 6796647]

19. Feldman AM, Ray PE, Silan CM, Mercer JA, Minobe W, Bristow MR. Selective gene expression in failing human heart. Quantification of steady-state levels of messenger RNA in endomyocardial biopsies using the polymerase chain reaction. Circulation 1991;83:1866–1872. [PubMed: 2040039]

20. Feldman AM, Weinberg EO, Ray PE, Lorell BH. Selective changes in cardiac gene expression during compensated hypertrophy and the transition to cardiac decompensation in rats with chronic aortic banding. Circulation Research 1993;73:184–192. [PubMed: 8508529]

21. Flesch M, Putz F, Schwinger RH, Bohm M. Functional relevance of an enhanced expression of the Na(+)-Ca2+ exchanger in the failing human heart. Ann N Y Acad Sci 1996;779:539–542. [PubMed: 8659874]

22. Flesch M, Schwinger RH, Schnabel P, Schiffer F, van Gelder I, Bavendiek U, Sudkamp M, Kuhn-Regnier F, Bohm M. Sarcoplasmic reticulum Ca2+ATPase and phospholamban mRNA and protein levels in end-stage heart failure due to ischemic or dilated cardiomyopathy. Journal of Molecular Medicine 1996;74:321–332. [PubMed: 8862513]

23. Frank JS, Mottino G, Reid D, Molday RS, Philipson KD. Distribution of the Na(+)-Ca2+ exchange protein in mammalian cardiac myocytes: an immunofluorescence and immunocolloidal gold-labeling study. J Cell Biol 1992;117:337–345. [PubMed: 1373142]

24. Gengo PJ, Sabbah HN, Steffen RP, Sharpe JK, Kono T, Stein PD, Goldstein S. Myocardial beta adrenoceptor and voltage sensitive calcium channel changes in a canine model of chronic heart failure. J Mol Cell Cardiol 1992;24:1361–1369. [PubMed: 1336065]

25. Go LO, Moschella MC, Watras J, Handa KK, Fyfe BS, Marks AR. Differential regulation of two types of intracellular calcium release channels during end-stage heart failure. J Clin Invest 1995;95:888–894. [PubMed: 7860772]

26. Gomez AM, Valdivia HH, Cheng H, Lederer MR, Santana LF, Cannell MB, McCune SA, Altschuld RA, Lederer WJ. Defective excitation-contraction coupling in experimental cardiac hypertrophy and heart failure [see comments]. Science 1997;276:800–806. [PubMed: 9115206]

27. Gruver EJ, Morgan JP, Stambler BS, Gwathmey JK. Uniformity of calcium channel number and isometric contraction in human right and left ventricular myocardium. Basic Research in Cardiology 1994;89:139–148. [PubMed: 8074638]

28. Gupta RC, Mishra S, Mishima T, Goldstein S, Sabbah HN. Reduced sarcoplasmic reticulum Ca(2+)-uptake and expression of phospholamban in left ventricular myocardium of dogs with heart failure. J Mol Cell Cardiol 1999;31:1381–1389. [PubMed: 10403755]

29. Hajjar RJ, Kang JX, Gwathmey JK, Rosenzweig A. Physiological effects of adenoviral gene transfer of sarcoplasmic reticulum calcium ATPase in isolated rat myocytes. Circulation 1997;95:423–429. [PubMed: 9008460]

30. Hajjar RJ, Schmidt U, Kang JX, Matsui T, Rosenzweig A. Adenoviral gene transfer of phospholamban in isolated rat cardiomyocytes. Rescue effects by concomitant gene transfer of sarcoplasmic reticulum Ca(2+)-ATPase. Circ Res 1997;81:145–153. [PubMed: 9242175]

31. Hasenfuss G, Reinecke H, Studer R, Meyer M, Pieske B, Holtz J, Holubarsch C, Posival H, Just H, Drexler H. Relation between myocardial function and expression of sarcoplasmic reticulum Ca(2+)-ATPase in failing and nonfailing human myocardium. Circulation Research 1994;75:434–442. [PubMed: 8062417]

32. He J, Conklin MW, Foell JD, Wolff MR, Haworth RA, Coronado R, Kamp TJ. Reduction in density of transverse tubules and L-type Ca(2+) channels in canine tachycardia-induced heart failure. Cardiovasc Res 2001;49:298–307. [PubMed: 11164840]

33. Hilgemann DW. Regulation and deregulation of cardiac Na(+)-Ca2+ exchange in giant excised sarcolemmal membrane patches. Nature 1990;344:242–245. [PubMed: 2314460]
34. Hobai IA, O'Rourke B. Decreased sarcoplasmic reticulum calcium content is responsible for defective excitation-contraction coupling in canine heart failure. Circulation 2001;103:1577–1584. [PubMed: 11257088]
35. Hobai IA, O'Rourke B. Enhanced Ca(2+)-activated Na(+)-Ca(2+) exchange activity in canine pacing-induced heart failure. Circ Res 2000;87:690–698. [PubMed: 11029405]
36. Ikemoto N, Ronjat M, Meszaros LG, Koshita M. Postulated role of calsequestrin in the regulation of calcium release from sarcoplasmic reticulum. Biochemistry 1989;28:6764–6771. [PubMed: 2790030]
37. Ito K, Yan X, Tajima M, Su Z, Barry WH, Lorell BH. Contractile reserve and intracellular calcium regulation in mouse myocytes from normal and hypertrophied failing hearts. Circ Res 2000;87:588–595. [PubMed: 11009564]
38. Jiang MT, Lokuta AJ, Farrell EF, Wolff MR, Haworth RA, Valdivia HH. Abnormal Ca2+ release, but normal ryanodine receptors, in canine and human heart failure. Circ Res 2002;91:1015–1022. [PubMed: 12456487]
39. Kääb S, Dixon J, Duc J, Ashen MD, Näbauer M, Beuckelmann DJ, McKinnon D, Tomaselli GF. Molecular basis of transient outward current downregulation in human heart failure: A decrease in Kv4.3 mRNA correlates with a reduction in current density. Circulation 1998;98:1383–1393. [PubMed: 9760292]
40. Kaab S, Nuss HB, Chiamvimonvat N, O'Rourke B, Pak PH, Kass DA, Marban E, Tomaselli GF. Ionic mechanism of action potential prolongation in ventricular myocytes from dogs with pacing-induced heart failure. Circ Res 1996;78:262–273. [PubMed: 8575070]
41. Kääb S, Nuss HB, Chiamvimonvat N, O'Rourke B, Pak PH, Kass DA, Marban E, Tomaselli GF. Ionic mechanism of action potential prolongation in ventricular myocytes from dogs with pacing induced heart failure. Circ Res 1996;78:262–273. [PubMed: 8575070]
42. Kaprielian RR, Stevenson S, Rothery SM, Cullen MJ, Severs NJ. Distinct patterns of dystrophin organization in myocyte sarcolemma and transverse tubules of normal and diseased human myocardium. Circulation 2000;101:2586–2594. [PubMed: 10840009]
43. Kawamura K, Kashii C, Imamura K. Ultrastructural changes in hypertrophied myocardium of spontaneously hypertensive rats. Jpn Circ J 1976;40:1119–1145. [PubMed: 136527]
44. Kimura J, Miyamae S, Noma A. Identification of sodium-calcium exchange current in single ventricular cells of guinea-pig. J Physiol 1987;384:199–222. [PubMed: 2443659]
45. Kiss E, Ball NA, Kranias EG, Walsh RA. Differential changes in cardiac phospholamban and sarcoplasmic reticular Ca(2+)-ATPase protein levels.Effects on Ca2+ transport and mechanics in compensated pressure-overload hypertrophy and congestive heart failure. Circulation Research 1995;77:759–764. [PubMed: 7554123]
46. Kiuchi K, Shannon RP, Komamura K, Cohen DJ, Bianchi C, Homcy CJ, Vatner SF, Vatner DE. Myocardial beta-adrenergic receptor function during the development of pacing-induced heart failure. J Clin Invest 1993;91:907–914. [PubMed: 8383704]
47. Kuo TH, Tsang W, Wang KK, Carlock L. Simultaneous reduction of the sarcolemmal and SR calcium ATPase activities and gene expression in cardiomyopathic hamster. Biochim Biophys Acta 1992;1138:343–349. [PubMed: 1532912]
48. Leri A, Liu Y, Malhotra A, Li Q, Stiegler P, Claudio PP, Giordano A, Kajstura J, Hintze TH, Anversa P. Pacing-induced heart failure in dogs enhances the expression of p53 and p53-dependent genes in ventricular myocytes. Circulation 1998;97:194–203. [PubMed: 9445173]
49. Levitsky DO, Nicoll DA, Philipson KD. Identification of the high affinity Ca(2+)-binding domain of the cardiac Na(+)-Ca2+ exchanger. J Biol Chem 1994;269:22847–22852. [PubMed: 8077237]
50. Li GR, Lau CP, Ducharme A, Tardif JC, Nattel S. Transmural action potential and ionic current remodeling in ventricles of failing canine hearts. Am J Physiol Heart Circ Physiol 2002;283:H1031–H1041. [PubMed: 12181133]
51. Li S, Margulies KB, Cheng H, Houser SR. Calcium current and calcium transients are depressed in failing human ventricular myocytes and recover in patients supported with left ventricular assist devices. (Abstract). Circulation 1999;100:I60.

52. Linck B, Boknik P, Eschenhagen T, Muller FU, Neumann J, Nose M, Jones LR, Schmitz W, Scholz H. Messenger RNA expression and immunological quantification of phospholamban and SR-Ca(2+)-ATPase in failing and nonfailing human hearts. Cardiovascular Research 1996;31:625–632. [PubMed: 8689655]
53. Lindner M, Brandt MC, Sauer H, Hescheler J, Bohle T, Beuckelmann DJ. Calcium sparks in human ventricular cardiomyocytes from patients with terminal heart failure. Cell Calcium 2002;31:175–182. [PubMed: 12027382]
54. Litwin SE, Bridge JH. Enhanced Na(+)-Ca2+ exchange in the infarcted heart. Implications for excitation-contraction coupling. Circulation Research 1997;81:1083–1093. [PubMed: 9400390]
55. Louch WE, Bito V, Heinzel FR, Macianskiene R, Vanhaecke J, Flameng W, Mubagwa K, Sipido KR. Reduced synchrony of Ca2+ release with loss of T-tubules-a comparison to Ca2+ release in human failing cardiomyocytes. Cardiovasc Res 2004;62:63–73. [PubMed: 15023553]
56. Luchner A, Stevens TL, Borgeson DD, Redfield MM, Bailey JE, Sandberg SM, Heublein DM, Burnett JC Jr. Angiotensin II in the evolution of experimental heart failure. Hypertension 1996;28:472–477. [PubMed: 8794835]
57. Marx SO, Gaburjakova J, Gaburjakova M, Henrikson C, Ondrias K, Marks AR. Coupled gating between cardiac calcium release channels (ryanodine receptors). Circ Res 2001;88:1151–1158. [PubMed: 11397781]
58. Marx SO, Reiken S, Hisamatsu Y, Jayaraman T, Burkhoff D, Rosemblit N, Marks AR. PKA phosphorylation dissociates FKBP12.6 from the calcium release channel (ryanodine receptor): defective regulation in failing hearts. Cell 2000;101:365–376. [PubMed: 10830164]
59. Mercadier JJ, Lompre AM, Duc P, Boheler KR, Fraysse JB, Wisnewsky C, Allen PD, Komajda M, Schwartz K. Altered sarcoplasmic reticulum Ca2(+)-ATPase gene expression in the human ventricle during end-stage heart failure. Journal of Clinical Investigation 1990;85:305–309. [PubMed: 2136864]
60. Mewes T, Ravens U. L-type calcium currents of human myocytes from ventricle of non-failing and failing hearts and from atrium. J Mol Cell Cardiol 1994;26:1307–1320. [PubMed: 7869391]
61. Meyer M, Bluhm WF, He H, Post SR, Giordano FJ, Lew WY, Dillmann WH. Phospholamban-to-SERCA2 ratio controls the force-frequency relationship. Am J Physiol 1999;276:H779–H785. [PubMed: 10070059]
62. Meyer M, Schillinger W, Pieske B, Holubarsch C, Heilmann C, Posival H, Kuwajima G, Mikoshiba K, Just H, Hasenfuss G. Alterations of sarcoplasmic reticulum proteins in failing human dilated cardiomyopathy. Circulation 1995;92:778–784. [PubMed: 7641356]
63. Movsesian MA, Bristow MR, Krall J. Ca2+ uptake by cardiac sarcoplasmic reticulum from patients with idiopathic dilated cardiomyopathy. Circ Res 1989;65:1141–1144. [PubMed: 2551528]
64. Movsesian MA, Karimi M, Green K, Jones LR. Ca(2+)-transporting ATPase, phospholamban, and calsequestrin levels in nonfailing and failing human myocardium. Circulation 1994;90:653–657. [PubMed: 8044934]
65. O'Rourke B, Kaab S, Kass DA, Tomaselli GF, Marban E. Role of Ca^{2+}-activated Cl^{-} current in shaping the action potential of canine ventricular myocytes from normal and failing hearts. Biophysical J 1996;70:A373.
66. O'Rourke B, Kass DA, Tomaselli GF, Kaab S, Tunin R, Marban E. Mechanisms of altered excitation-contraction coupling in canine tachycardia-induced heart failure, I: experimental studies. Circ Res 1999;84:562–570. [PubMed: 10082478]
67. Pak PH, Nuss HB, Tunin RS, Kaab S, Tomaselli GF, Marban E, Kass DA. Repolarization abnormalities, arrhythmia and sudden death in canine tachycardia-induced cardiomyopathy. J Am Coll Cardiol 1997;30:576–584. [PubMed: 9247535]
68. Pogwizd SM, Qi M, Yuan W, Samarel AM, Bers DM. Upregulation of Na(+)/Ca(2+) exchanger expression and function in an arrhythmogenic rabbit model of heart failure. Circ Res 1999;85:1009–1019. [PubMed: 10571531]
69. Rasmussen RP, Minobe W, Bristow MR. Calcium antagonist binding sites in failing and nonfailing human ventricular myocardium. Biochem Pharmacol 1990;39:691–696. [PubMed: 2154992]
70. Reinecke H, Studer R, Vetter R, Holtz J, Drexler H. Cardiac Na+/Ca2+ exchange activity in patients with end-stage heart failure. Cardiovasc Res 1996;31:48–54. [PubMed: 8849588]

71. Satoh H, Blatter LA, Bers DM. Effects of [Ca2+]i, SR Ca2+ load, and rest on Ca2+ spark frequency in ventricular myocytes. Am J Physiol 1997;272:H657–H668. [PubMed: 9124422]
72. Schroeder F, Handrock R, Beuckelmann DJ, Hirt S, Hullin R, Priebe L, Schwinger RHG, Weil J, Herzig S. Increased availability and open probability of single L-type calcium channels from failing compared with nonfailing human ventricle. Circulation 1998;98:969–976. [PubMed: 9737516]
73. Schwinger RH, Bohm M, Schmidt U, Karczewski P, Bavendiek U, Flesch M, Krause EG, Erdmann E. Unchanged protein levels of SERCA II and phospholamban but reduced Ca2+ uptake and Ca(2+)-ATPase activity of cardiac sarcoplasmic reticulum from dilated cardiomyopathy patients compared with patients with nonfailing hearts. Circulation 1995;92:3220–3228. [PubMed: 7586307]
74. Schwinger RH, Munch G, Bolck B, Karczewski P, Krause EG, Erdmann E. Reduced Ca(2+)-sensitivity of SERCA 2a in failing human myocardium due to reduced serin-16 phospholamban phosphorylation. J Mol Cell Cardiol 1999;31:479–491. [PubMed: 10198180]
75. Shannon TR, Pogwizd SM, Bers DM. Elevated sarcoplasmic reticulum Ca2+ leak in intact ventricular myocytes from rabbits in heart failure. Circ Res 2003;93:592–594. [PubMed: 12946948]
76. Shorofsky SR, Aggarwal R, Corretti M, Baffa JM, Strum JM, Al-Seikhan BA, Kobayashi YM, Jones LR, Wier WG, Balke CW. Cellular mechanisms of altered contractility in the hypertrophied heart: big hearts, big sparks. Circ Res 1999;84:424–434. [PubMed: 10066677]
77. Sipido KR, Stankovicova T, Flameng W, Vanhaecke J, Verdonck F. Frequency dependence of Ca2+ release from the sarcoplasmic reticulum in human ventricular myocytes from end-stage heart failure. Cardiovasc Res 1998;37:478–488. [PubMed: 9614502]
78. Studer R, Reinecke H, Bilger J, Eschenhagen T, Bohm M, Hasenfuss G, Just H, Holtz J, Drexler H. Gene expression of the cardiac Na(+)-Ca2+ exchanger in end-stage human heart failure. Circ Res 1994;75:443–453. [PubMed: 8062418]
79. Takahashi T, Allen PD, Lacro RV, Marks AR, Dennis AR, Schoen FJ, Grossman W, Marsh JD, Izumo S. Expression of dihydropyridine receptor (Ca2+ channel) and calsequestrin genes in the myocardium of patients with end-stage heart failure. J Clin Invest 1992;90:927–935. [PubMed: 1326001]
80. Tsuji Y, Opthof T, Kamiya K, Yasui K, Liu W, Lu Z, Kodama II. Pacing-induced heart failure causes a reduction of delayed rectifier potassium currents along with decreases in calcium and transient outward currents in rabbit ventricle. Cardiovasc Res 2000;48:300–309. [PubMed: 11054476]
81. Vatner DE, Sato N, Kiuchi K, Shannon RP, Vatner SF. Decrease in myocardial ryanodine receptors and altered excitation-contraction coupling early in the development of heart failure. Circulation 1994;90:1423–1430. [PubMed: 7522133]
82. Wier WG, Balke CW, Michael JA, Mauban JR. A custom confocal and two-photon digital laser scanning microscope. Am J Physiol Heart Circ Physiol 2000;278:H2150–H2156. [PubMed: 10843915]
83. Wolff MR, de Tombe PP, Harasawa Y, Burkhoff D, Bier S, Hunter WC, Gerstenblith G, Kass DA. Alterations in left ventricular mechanics, energetics, and contractile reserve in experimental heart failure. Circ Res 1992;70:516–529. [PubMed: 1311222]
84. Yoshiyama M, Takeuchi K, Hanatani A, Kim S, Omura T, Toda I, Teragaki M, Akioka K, Iwao H, Yoshikawa J. Differences in expression of sarcoplasmic reticulum Ca2+-ATPase and Na+-Ca2+ exchanger genes between adjacent and remote noninfarcted myocardium after myocardial infarction. J Mol Cell Cardiol 1997;29:255–264. [PubMed: 9040040]
85. Zarain-Herzberg A, Afzal N, Elimban V, Dhalla NS. Decreased expression of cardiac sarcoplasmic reticulum Ca(2+)-pump ATPase in congestive heart failure due to myocardial infarction. Molecular & Cellular Biochemistry 1996;164:285–290. [PubMed: 8974068]

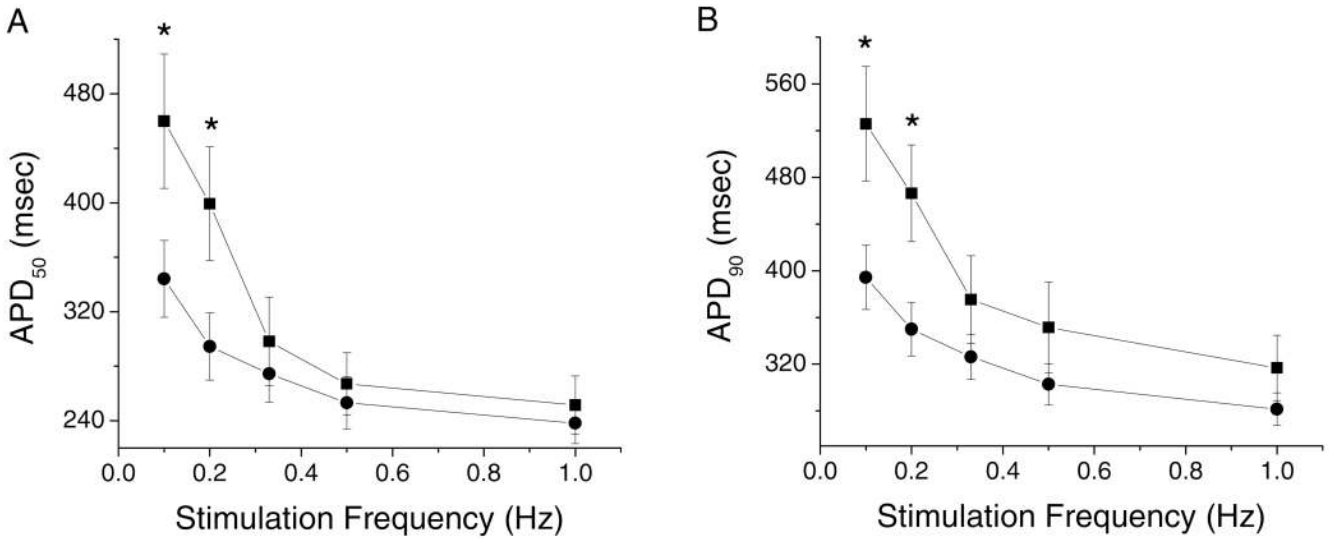

Figure 1.

Stimulation frequency dependent differences in the action potential (AP) duration (APD) and membrane resting potential of ventricular myocytes isolated from control and failing ventricles (N_c=12, n_c=18; N_f=5, $n_{f=}$11). (A). APD at 50% repolarization (APD_{50}). (B). APD at 90% repolarization (APD_{90}). There is an overall prolongation of AP duration of myocytes isolated from failing compared to control hearts. In this and all subsequent figures circles represent data from control and squares from failing hearts. Mean ± SE, *p<0.05 vs. control.

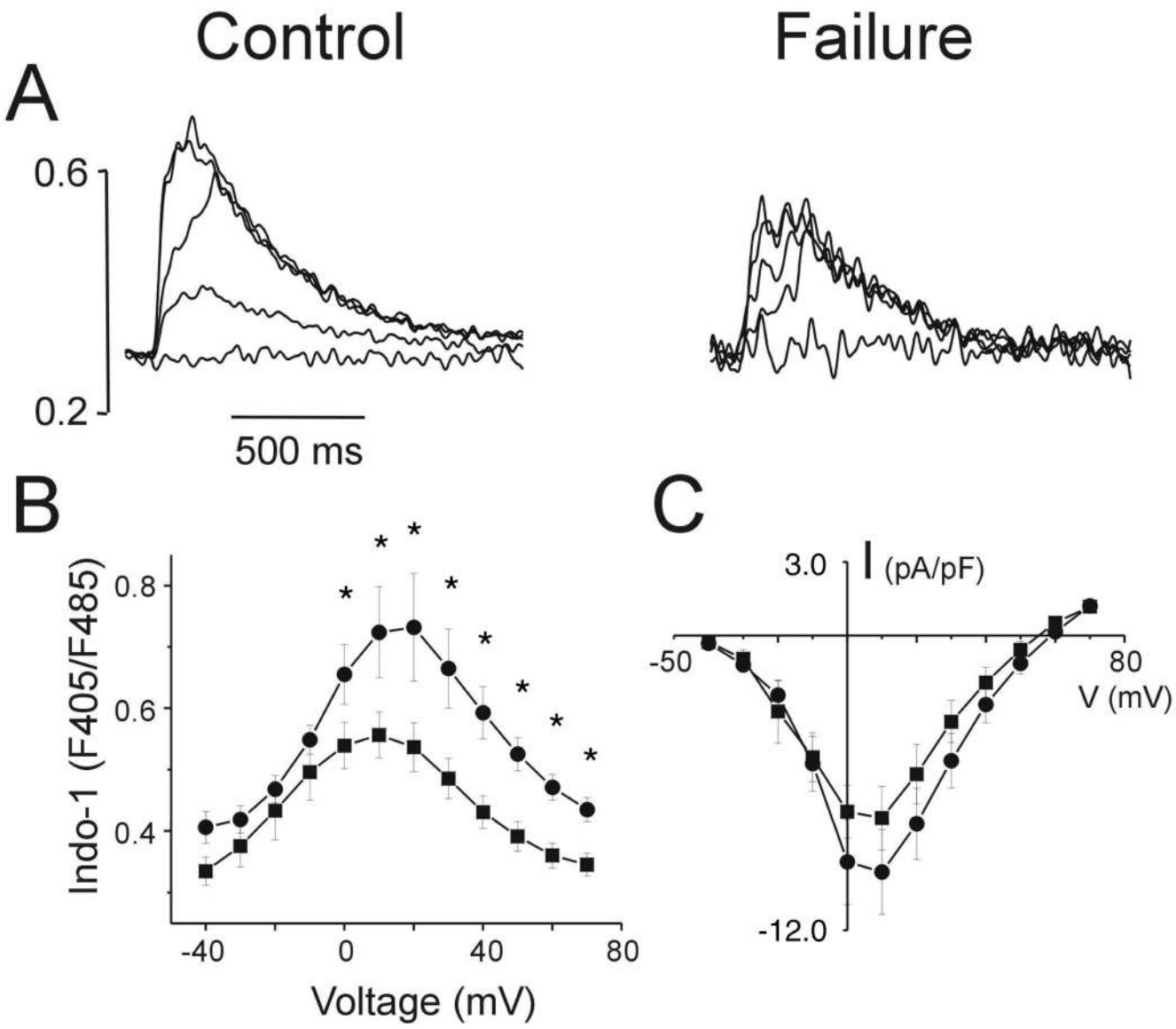

Figure 2.

Records of representative intracellular Ca^{2+} transients (Indo-1 fluorescent ratios 405/485 nm) from control and failing hearts (A), elicited by voltage steps to −40, −20, 0, 20 and 40 mV from a holding voltage of −80 mV. Summary Ca^{2+} transient data are shown in panel B (* $p<0.05$ failing vs. control). Peak I-V relations for the L-type Ca^{2+} currents are shown in panel C.

A

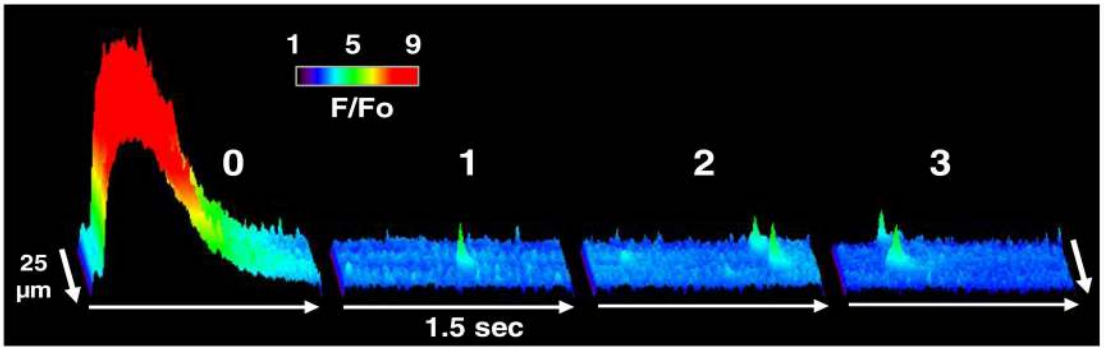

B

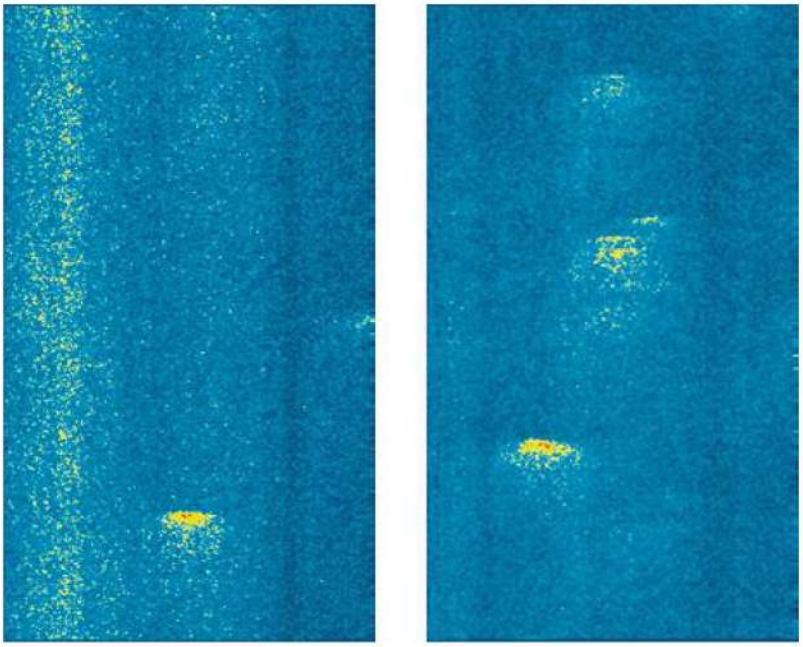

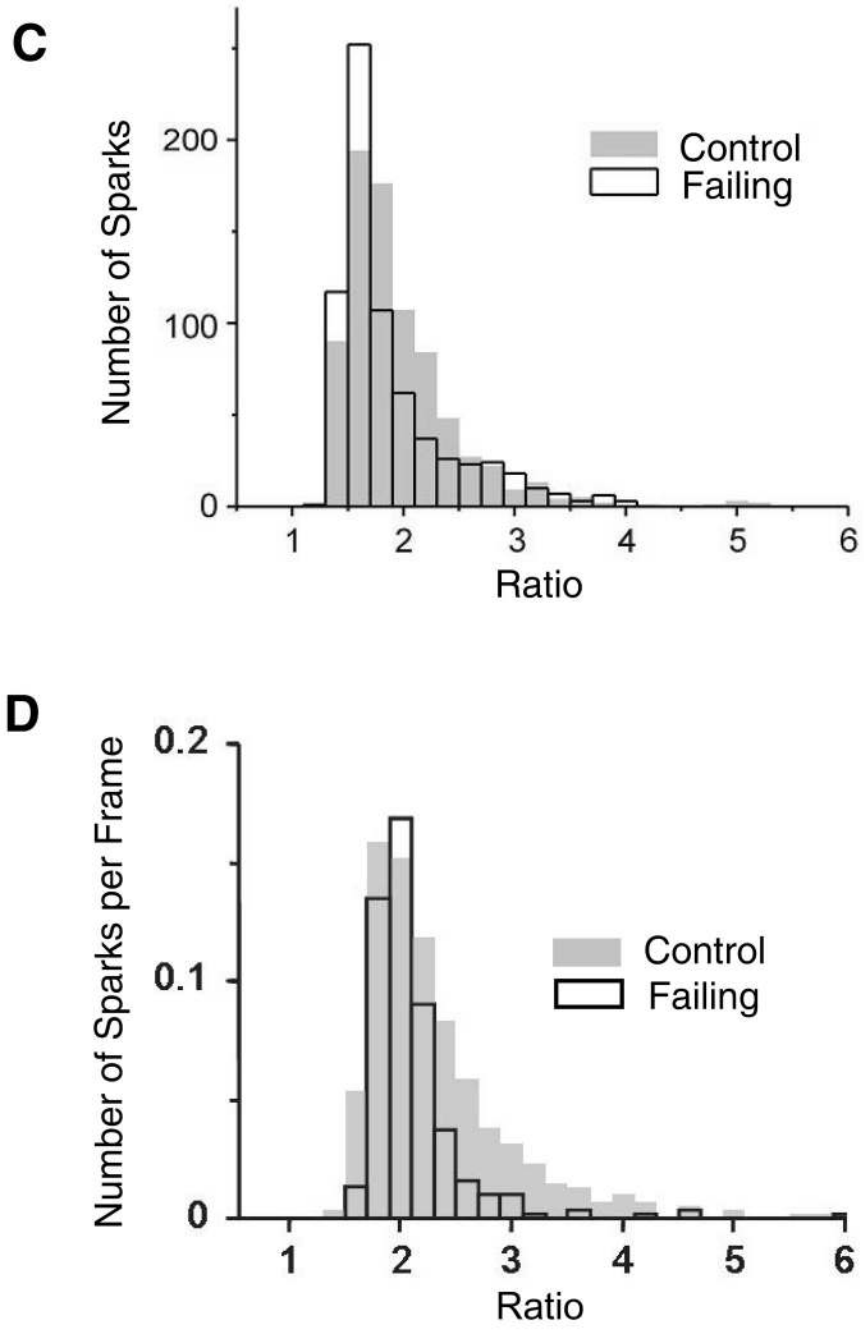

Figure 3.

Local SR-Ca^{2+} release events (Ca^{2+}-sparks) in rabbit ventricular myocytes from control and failing animals. (A) 3D representation of spatiotemporal variations of $[Ca^{2+}]_i$ along a 25μm line scan during ~ 9 seconds. Each frame represents a series of 500 successive scans (3ms/scan; 1.5s/frame); the number of scans was translated into horizontal time scale (horizontal arrow). Ca^{2+} sparks were sampled during the resting period (Frames 1, 2 and 3) following the stimulated twitch (Frame 0). Variations of the ratio of fluorescence intensities F/Fo reflected the local variations of $[Ca^{2+}]_i$ as indicated by the pseudo-color bar (see text). (B). Representative sparks in cells isolated from control (left) and failing (right) hearts, respectively.

(C) Distribution of the amplitudes of the Ca^{2+} sparks as reflected in the ratio between peak and background. The Ca^{2+} sparks from the failing animals are smaller than the Ca^{2+} sparks from the control animals ($p<0.0001$, Mann-Whitney test of medians). (D) Comparison of the frequency distribution of spark amplitudes in myocytes from control and failing hearts showed that the two distributions were not statistically different (total number of observations was 474 and 289 in myocytes from control and failing hearts respectively).

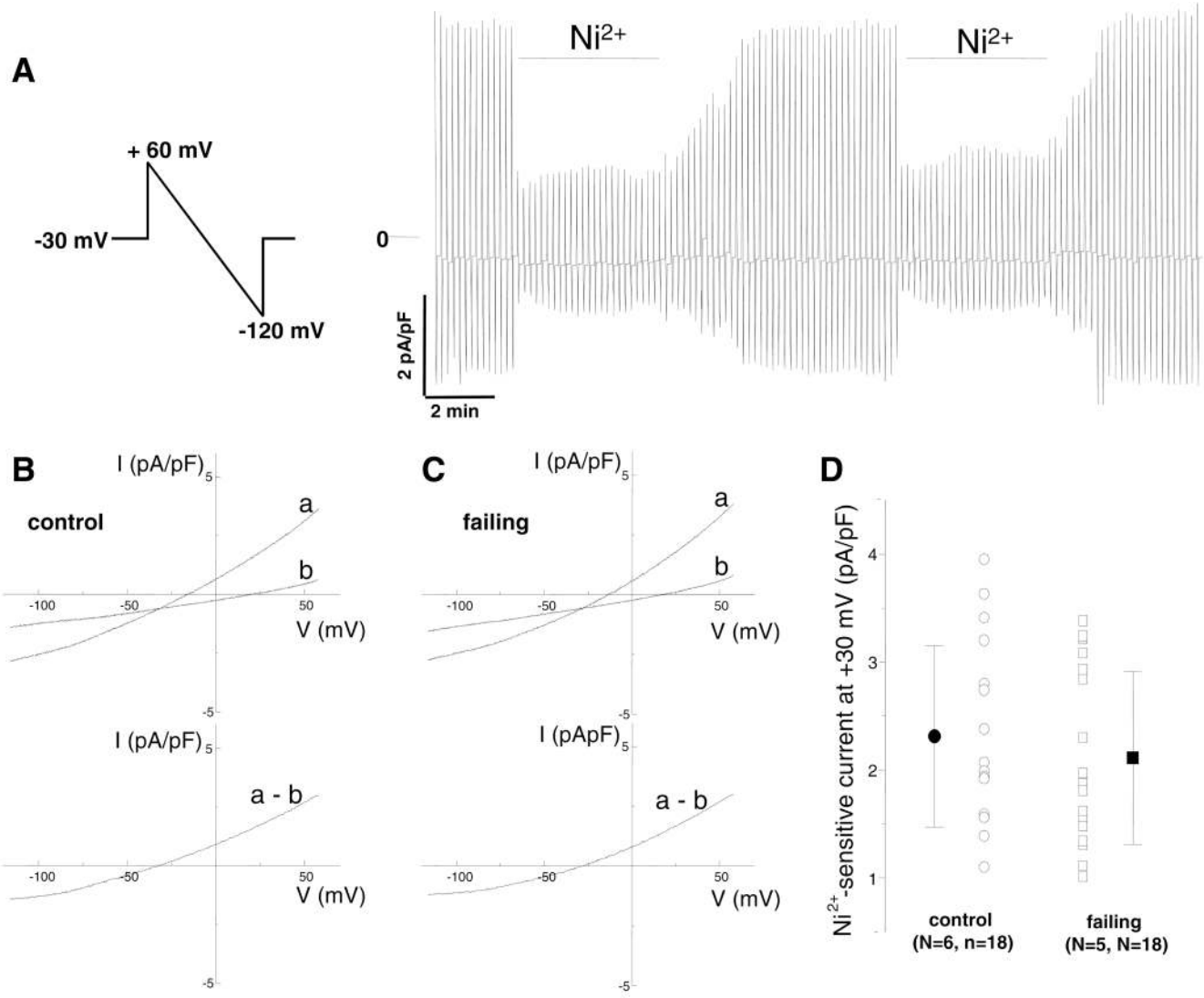

Figure 4.

Measurement of Ni^{2+}-sensitive Na^{+}-Ca^{2+} exchanger current density in rabbit ventricular myocytes. (A) Representative current records shown on a slow time scale elicited by the ramp protocol shown (+60 to −120 mV, 90 mV/s, 0.1 Hz, holding at −30 mV). The horizontal bars depict application of 5 mmol/L Ni^{2+}. Note the rapid time course of the Ni^{2+}-induced block, the reproducibility of the Ni^{2+}-insensitive component, and the relative stability of recording without significant rundown. Measurement of Ni^{2+}-sensitive Na^{+}-Ca^{2+} exchanger current density in rabbit ventricular myocytes isolated from control (B) and failing (C) hearts (top). Representative current traces were elicited by the same ramp protocol used in panel A. Current-voltage relationships before (a) and after (b) application of 5 mmol/L Ni^{2+}. (bottom) The difference is the Na^{+}-Ca^{2+} exchanger current. (D) There were no differences in the Ni^{+}-sensitive current in myocytes isolated from control and failing hearts.

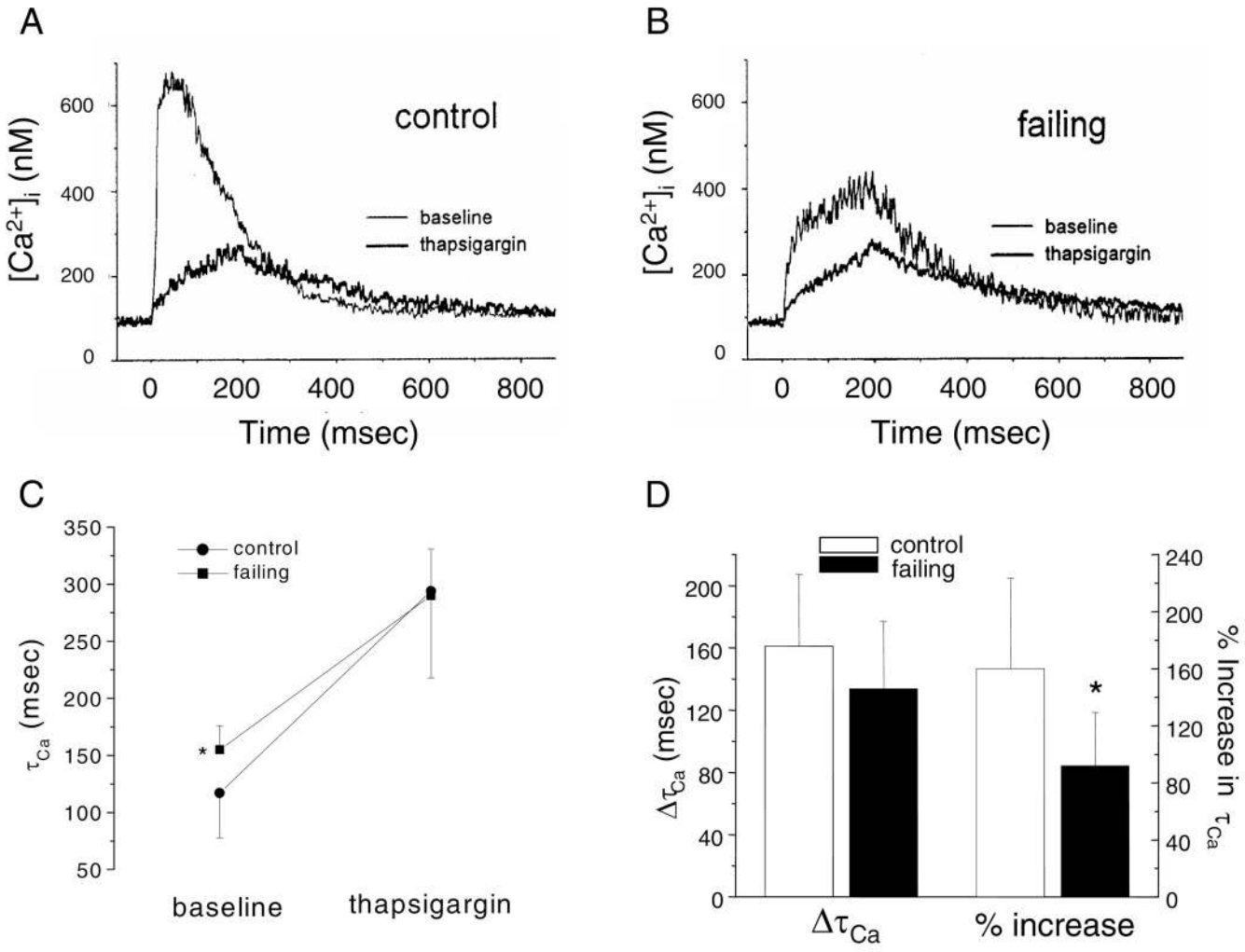

Figure 5.

Effect of SR Ca^{2+}-ATPase inhibition on Ca^{2+} transients ($[Ca^{2+}]_i$). (A), (B): $[Ca^{2+}]_i$ were evoked by 200 msec voltage-clamp steps to +20 mV from a holding potential of −80 mV at a rate of 0.5 Hz in rabbit ventricular myocytes isolated from control (A) and failing (B) ventricular myocardium in the absence and presence of 10 μmol/L thapsigargin. (C) The summarized data (control: N=3 animals, n=13 myocytes; failing: N=3, n=16) demonstrate a substantial increase in the time constant of Ca^{2+} removal from the myocyte (τ_{Ca}) in myocytes isolated from failing compared to control ventricles under baseline conditions. Blocking the Ca^{2+}-ATPase with thapsigargin, however increased the absolute τ_{Ca} to a comparable value in both groups. (D) There was a slightly but not statistically significant larger increase in τ_{Ca} in the control group. The relative increase in τ_{Ca} with thapsigargin was significantly larger in the control compared to failing myocardium (*p<;0.05).

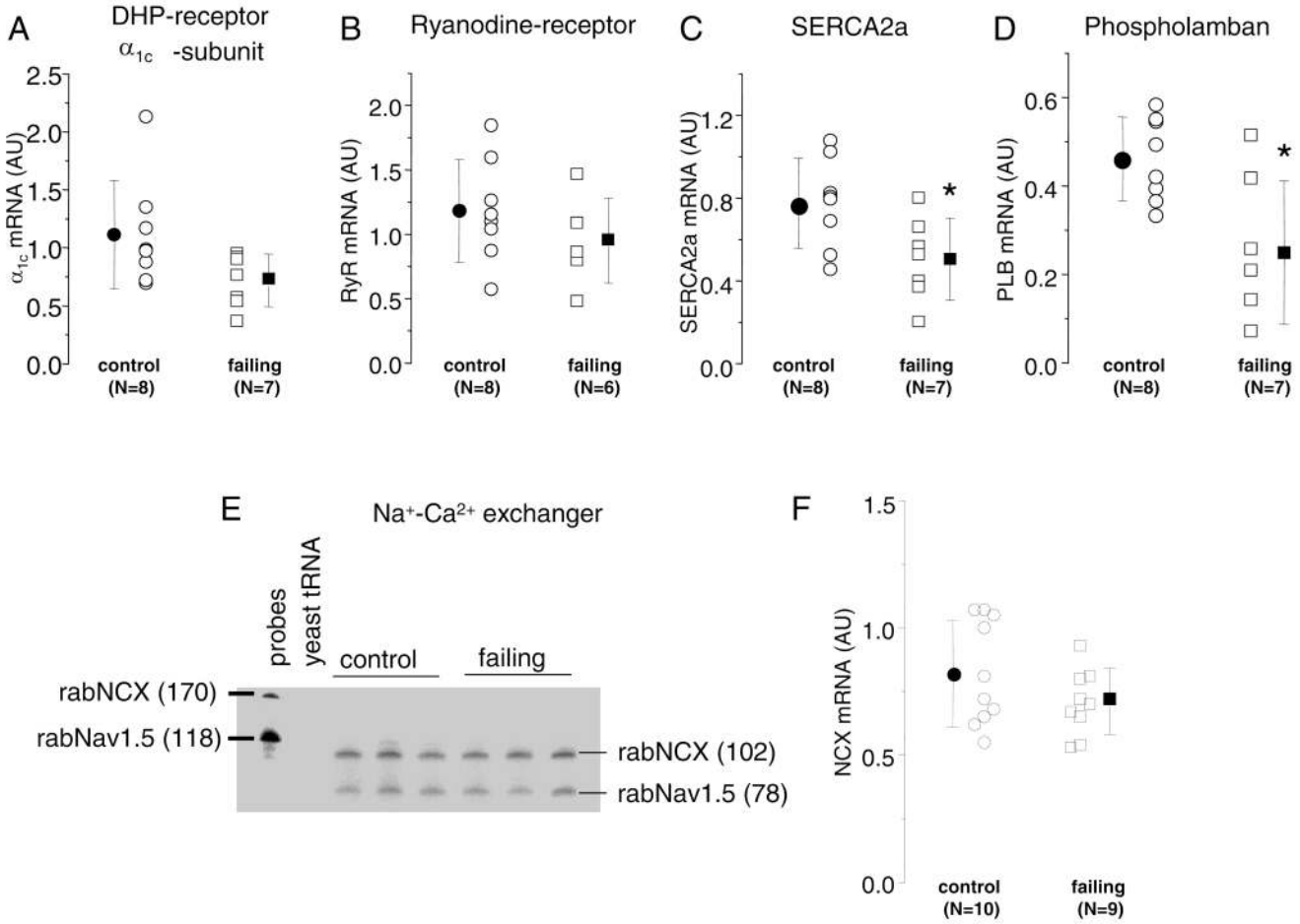

Figure 6.

mRNA levels of Ca^{2+} handling proteins in control and failing hearts. (A–D). Scatter plots of normalized α_{1c} (A), RyR2 (B), SERCA2a (C), PLB (D) mRNA in control and failing hearts measured by kinetic RT-PCR. The steady-state levels of α_{1c} and RyR2 mRNAs are not altered in the failing compared to the control hearts, while SERCA2a and PLB are significantly decreased in the failing heart. (E) Representative NCX RPA showing the expected bands for the NCX (probe 180 bp, protected fragment 118 bp) and the cardiac Na channel (Nav1.5, probe 170 bp, protected fragment 78 bp) in control and failing hearts. The first lane (P) contains the probes alone and the lane marked t, yeast tRNA and the next six lanes are 10 μg of total RNA from different control and failing ventricles. (F) Scatter plot of normalized NCX mRNA in 10 control and 9 failing hearts, the values plotted are the average of duplicate determinations; the steady-state level of mRNA encoding NCX is not altered in failing compared to control hearts (AU, Arbitrary Units and *$p < 0.05$).

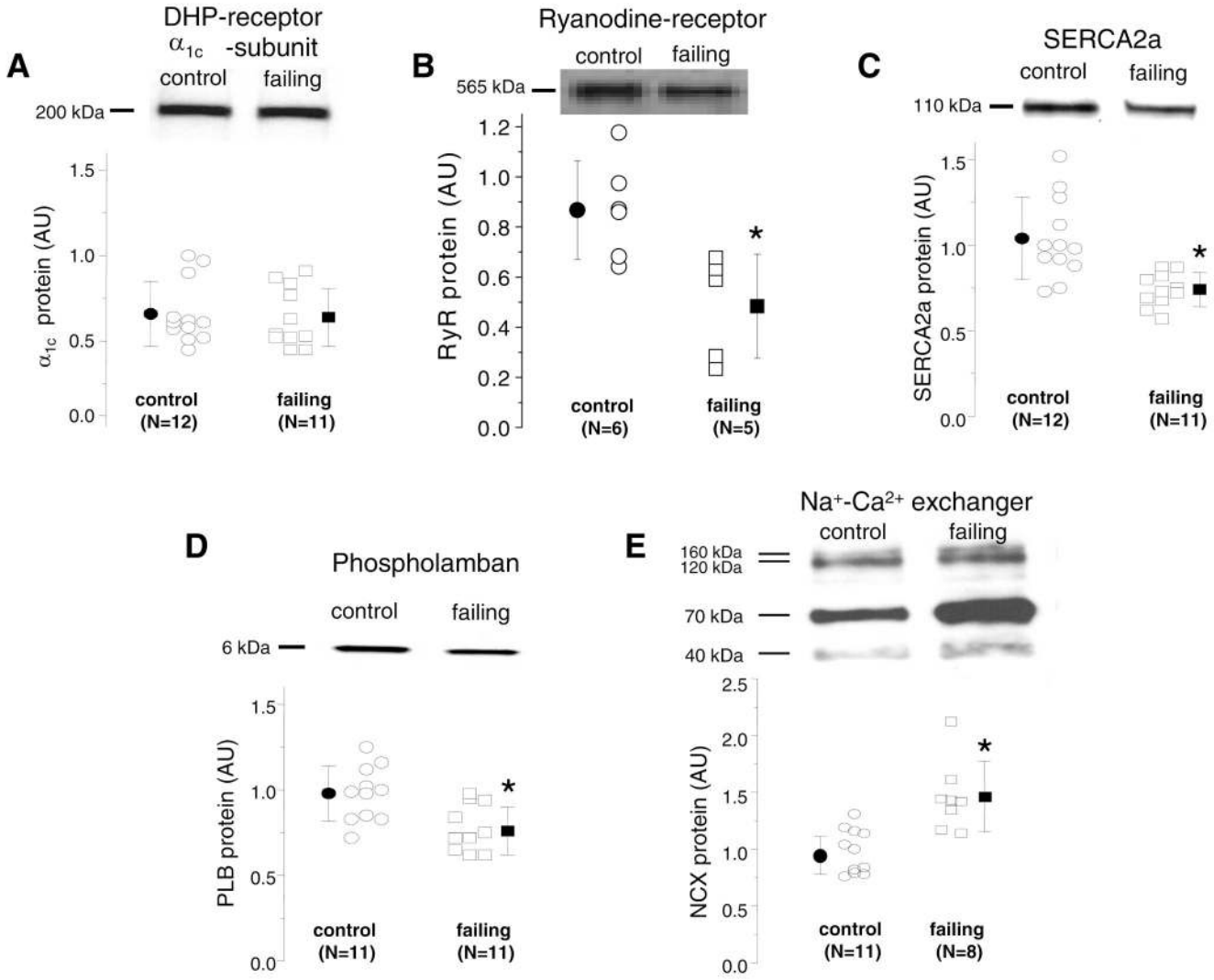

Figure 7.

Protein levels of the major calcium handling proteins in control and failing hearts. Representative Western blots and scatter plots of the α_{1c} subunit of the Ca channel (A), RyR (B), SERCA2a (C), PLB (D), NCX (E) in control and failing hearts. Scatter plots for each of the Ca^{2+} handling proteins demonstrate a significant down regulation of immunoreactive RyR, SERCA2a, PLB monomer and an up regulation of NCX. There is no change in immunoreactive α_{1c} (A). (AU, Arbitrary Units and *$p < 0.05$).

Table 1

Riboprobe amplification and RT-PCR Primers and Probes.

Transcript	Probe/Primers
Ribprobes	
rabH1	forward 5’ GGG AGA GCG AGA GCC ACC
	reverse 5’ GTG GAC TGC AAT GGG GTG G
rabNCX	forward 5’ TGT CTG TCA TTG AAG TGT GTG G,
	reverse 5’ AAT CTT CCT CGT CTC TCC ATC
RT-PCR	
rabα_{1c}	probe 5’ 6FAMCTA CCA AAG TGA CAG CCG GAG CGCTAMRA 3’
	forward 5’ CCT GTT TGG CAA CCA TGT CA 3’
	reverse 5’ GTG GGC GCT GCG TAG TG 3’
rabSERCA2a	probe 5’ 6FAMCTC CAA CGA GTT ACC GGC TGA AGA AGTAMRA 3’
	forward 5’ GGT CAA GAA GCT CAA GGA GAG ATG 3’
	reverse 5’ CAA TCA CAA GTT CCA GCA AGG TT 3’
rabRyR	probe 5’ 6FAMCAC TGG ACG TGG CAG CCT CTAMRA 3’
	forward 5’ CAC CAG CTA TGA GAG GTT CAA CA 3’
	reverse 5’ GCT AGG GCC AAC TCA TTA TTA TCC 3’
rabPLB	probe 5’ 6FAMCAG AAC CTA TTT ATC AAT TTC TGT CTC ATTAMRA 3’
	forward 5’ CTC AAC AAG CAC GTC AAA ACC T 3’
	reverse 5’ GCA GAT CAG CAG GAG ACA TAT CA 3’

Table 2

Current densities of sodium calcium exchanger at selected voltages and reversal potentials in myocytes isolated from control and failing ventricular myocytes.

	−115 mV	−90 mV	−60 mV	−30 mV	0 mV	30 mV	60 mV
total current (before Ni^{2+})							
Control	−3.78±1.84	−3.15±1.51	−2.16±1.05	−0.86±0.47	0.70±0.27	2.59±1.03	4.66±1.93
Failing	−3.55±3.57	−3.34±2.07	−2.27±1.36	−0.95±0.64	0.57±0.43	2.49±1.22	4.35±2.07
Ni^{2+}-insensitive current (background current)							
Control	−1.88±0.86	−1.52±0.72	−1.20±0.54	−0.78±0.36	−0.32±0.16	0.29±0.25	1.00±0.59
Failing	−2.37±1.64	−1.87±1.28	−1.40±0.85	−0.86±0.44	−0.31±0.22	0.38±0.66	1.09±1.13
Ni^{2+}-sensitive current (Na^{+}-Ca^{2+} exchange current)							
Control	−1.90±1.03	−1.62±0.83	−0.97±0.55	−0.08±0.19	1.02±0.37	2.31±0.84	3.67±1.44
Failing	−1.76±1.13	−1.44±0.87	−0.81±0.53	−0.03±0.21	0.94±0.36	2.11±0.80	3.25±1.26

Control: N=6, n=18, C = 151±48 pF; failing: N=5, n=18, C = 160±47 pF. Values are Mean ± SD in pA/pF.